J. COMBIN. MATH. COMBIN. COMPUT. 127a (2025) 7983--8001

Journal of Combinatorial Mathematics and Combinatorial Computing
www.combinatorialpress.com/jcmcc

Combinatorial Press

A non-contact aircraft landing impact test spatial attitude and deformation measurement and analysis method

Zhaoming Huang[1,2,✉], Rui Hu[1], Chenchen Zhu[1,2]

[1] Aircraft Strength Research Institute of China, Xi'an, Shaanxi, 710000, China
[2] National Key Laboratory of Strength and Structural Integrity, Xi'an, Shaanxi, 710000, China

ABSTRACT
This paper designs the system structure to meet the impact test of aircraft landing, and utilizes finite element calculation to derive the maximum impact stress of the impact platform and the maximum bearing stress. Analyze the attitude combination measurement system, based on the coordinate transformation theory to build a digital level, attitude probe and inclination sensor combination of attitude measurement model, the horizontal attitude angle of the object to solve the calculation. And the robustness overall least squares method is applied for plane fitting. The overall flow of the attitude measurement experiment is designed to analyze the stability and accuracy of the spatial attitude measurement system based on the combination of multi-sensors, and analyze the measurement error of the measured target in different states (translation or deflection). Different attitude solving algorithms are used to measure the attitude angle of the dynamic simulation experiment, and the measurement errors of the roll angle, pitch angle, heading angle and the root-mean-square error are compared. The RMS errors of the roll angle, pitch angle and heading angle measured by the attitude solution model in this paper are 0.2982, 0.2214 and 1.0333, respectively.Comparing with the data in the charts and graphs, it can be seen that the measurement errors and RMS errors of the attitude solution algorithm used in this paper are smaller, which are more in line with the requirements of the target spatial attitude measurement.

Keywords: spatial attitude measurement, multi-sensor, attitude angle measurement, landing shock

1. Introduction

In recent years, China has successively promulgated programmatic documents, which put forward new requirements for the construction and development of civil aviation, and further breakthroughs in civil aviation infrastructure bottlenecks are still an important foundation to support a strong civil aviation country in the new era, and in order to ensure the safety of civil aviation airplanes, the landing impact

✉ Corresponding author.
E-mail address: hzmhzm14@qq.com (Z. Huang).
Received 20 February 2024; Revised 15 May 2024; Accepted 20 November 2024; Published Online 15 April 2025.
DOI: 10.61091/jcmcc127a-439

test is still an important method of inspection [1-4]. Aircraft landing impact test is a commonly used experimental method to test the performance and response of aircraft materials or structures when subjected to impact loads. Impact tests are designed to simulate real-world impact situations in order to assess the strength, durability and reliability of a material or structure [5-8].

The principles of impact testing can be summarized into two key aspects, impact load and material/structure response. Impact load is a sudden and instantaneous force applied to a material or structure. This force can be from a variety of sources such as falling objects, explosions, collisions, etc [9-12]. The magnitude, direction and duration of the impact load can have an effect on the response of the material or structure. The response of a material or structure is the deformation, damage, or other performance of an aircraft after being subjected to an impact load [13-15]. This response can be evaluated in various ways such as displacement, strain, stress, vibration, etc. By analyzing the response of a material or structure under impact loading, its performance and behavior can be better understood [16-18]. The experimental non-contact measurement is based on photoelectric, electromagnetic, ultrasonic and other technologies, in the case of the sensing element of the instrument is not in contact with the surface of the object to be measured, you can obtain a variety of external or intrinsic data characteristics of the object to be measured method, typical non-contact measurement methods, such as laser triangulation, eddy current method, ultrasonic measurement, machine vision measurement, etc. [19-22].

This paper analyzes the different stages of the aircraft landing process, and puts forward the design requirements for the impact platform, waveform generator, pendulum system, and guiding mechanism of the landing impact test system respectively. The finite element is used to check the payload, the maximum design load and the system strength of the landing impact test, and the simulation test calculates the maximum impact stress of the impact platform and the maximum bearing stress. Propose the space attitude measurement system based on the combination of multi-sensors, analyze the attitude solving process, and combine the least-squares method for plane fitting. Design the overall flow of the experiment and build the platform needed for the experiment. Analyze the stability and accuracy of the spatial attitude measurement system based on multi-sensor combination, and use the attitude solution model to measure the attitude angle of the target in the dynamic simulation test.

2. Landing impact tests and space attitude measurements

2.1. Analysis of aircraft landing process

In order to realize the refined dynamic simulation of the aircraft landing process, one should first have a clear and accurate understanding of the complete landing process.

When approaching for landing, starting at a safe altitude, the airplane drops the landing gear and slides down a nearly straight and oblique trajectory at a stable speed. The pilot starts to pull the stick when it is about 6~12m off the ground, increasing the pitch angle to level the airplane attitude. When the wheels are about 1 m above the ground, the pilot maintains deceleration and level flight until the lift is no longer able to balance the weight of the airplane. The airplane floats down under gravity and the main landing gear wheels are grounded.

When the speed is reduced to a certain level, the pilot pushes the stick to bring the front wheels to the ground for a three-point slip run, while using the deceleration device to continuously decelerate until the airplane safely stops moving.

The complete landing process of an airplane is the process of safely grounding until it stops after four staged operations of slipping, leveling, leveling deceleration, and drifting down, starting from the landing altitude, which can be approximated into the slipping deceleration stage, the drifting down stage, and the landing skidding stage.

2.2. Landing impact test system structure and simulation design

2.2.1. Design elements. The landing impact test system mainly includes the impact platform, waveform generator, pendulum system, guiding mechanism and other subsystems [23]. According to the airworthiness standards of the CAAC for transport aircraft, the design points of each sub-system include the following aspects.

1) Impact platform. The impact platform should meet the requirements of carrying large air transportation materials, as well as the requirements of impact overload during emergency landing, i.e., the landing impact test system should meet the structural strength requirements of maximum 16g impact overload.

2) Waveform generator. Waveform generator should ensure that the impact platform to achieve a certain impact speed and kinetic impact, impact overload waveform. Emergency landing conditions should include lateral 1.5g, heading 3g, 9g and 16g, the loading waveform should be a triangular wave, and the time point corresponding to the peak value of the load should appear after the specified time.

3) Pendulum system and guiding mechanism. The pendulum system shall be coordinated with the guiding mechanism to ensure that the impact velocity of 7.5m/s is achieved at the moment of impact between the impact platform and the waveform generator.

2.2.2. Impact platform simulation design. The impact platform consists mainly of a frame, steel plate, impact headstock, screws and retaining rings. Among them, the frame and steel plate are used to carry air transport materials, the impact head frame is used to hit the waveform generator and carry the impact force, and the screws and retaining ring are used to retain and fix the air transport materials.

In order to ensure that the rigidity of the impact platform to meet the requirements, the frame is made of square steel welded, covered with steel plate, steel plate and frame connection parts using the lower part of the riveting welding to ensure that the upper surface is flat. The impact head frame is used to directly impact the waveform generator, transfer the collision force to the longitudinal frame, and then transferred to the air cargo through the steel plate and the tether ring.

According to the current carrying capacity of the air transportation platform, the designed mass of the impact platform is about 10t, and the mass of the air transportation material is about 15t, with a total mass of about 25t. Since the heading impact 16g is the worst working condition among the four emergency landing conditions, the heading impact 16g is selected for the finite element calibration of the impact platform. According to the finite element calibration, multiplying 25 t by 16g, the payload is 400t, and according to the design of 1.25 times the safety factor, the maximum design load is up to 500t.

With static finite element calibration of the strength of the nuclear test system, the impact platform material is Q345 steel, and the maximum yield strength is 345 MPa. Under the static general module of ABAQUS, the platform is divided into 163510 tetrahedral meshes, and the modulus of elasticity of the material and the Poisson's ratio are 210,000 Pa and 0.3 respectively.

According to the calculation, the maximum inertia force of the platform is about 3200kN. During the test, the waveform generator transfers the impact load to the platform through the impact head frame, and the platform transfers it to the test piece through the tether system. Therefore, the static calibration takes the maximum impact force of 3200kN load is applied to the platform impact head frame, and the displacement constraint is applied to the tail end of the impact platform as 0, and the finite element calculation is carried out.

For the impact calibration, the maximum impact stress of the platform is about 250MPa, and according to the load bearing calibration, the maximum load bearing stress of the main beam of the frame is about 240MPa. According to the simulation, the impact stress and load bearing stress do not exceed the yield point of the material, which is considered to be the transient impact load. Therefore, the impact platform can meet the requirements of load bearing and the impact overload requirements during emergency landing.

2.3. *Space Attitude Measurement System Based on Multi-Sensor Combination*

2.3.1. Combined Attitude Measurement System. The spatial attitude combination measurement system is shown in Fig. 1, which is mainly composed of digital level, dual-axis inclination sensor, attitude probe, five-degree-of-freedom adjustment platform, single-degree-of-freedom attitude adjustment mechanism, convenient computer, and data acquisition and processing software.

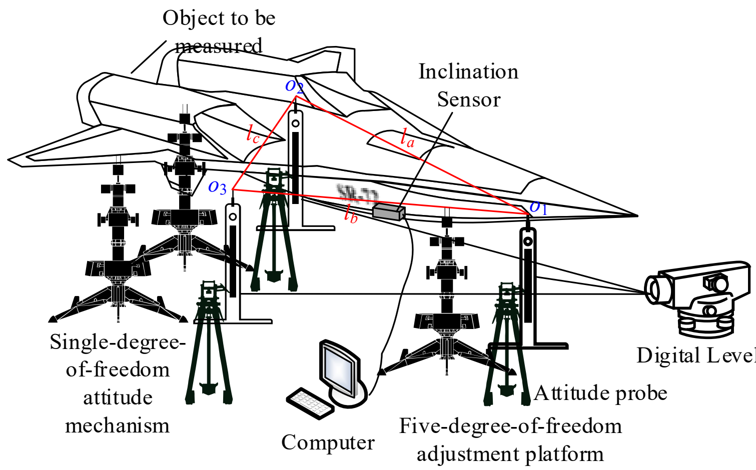

Fig. 1. Spatial attitude combination measurement system

During attitude measurement and adjustment, the attitude of the object can be defined by the transformation relationship between coordinate systems [24]. The coordinate transformation from the object coordinate system to the reference coordinate system is shown in Fig. 2, and the reference coordinate system is $ox_wy_wz_w$ and the object coordinate system is $ox_ty_tz_t$. The rotation angles α, β, and γ are defined as the object's pitch, roll, and yaw angles, respectively, which are positive in the counterclockwise direction and negative in the clockwise direction when viewed along the positive direction of the coordinate axes.

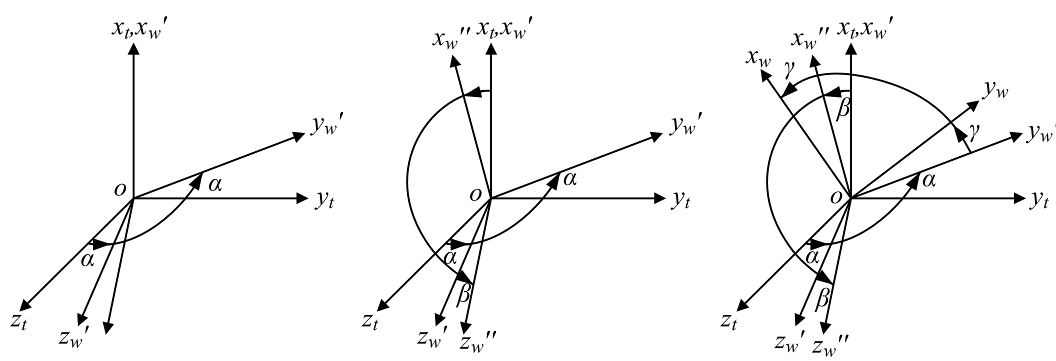

Fig. 2. Coordinate transformation of object coordinates to reference coordinates

In this paper, the spatial transformation between two coordinate systems is represented in the order of rotation around $x-y-z$ in sequence. Assuming that the reference coordinate system $ox_wy_wz_w$ coincides with the object coordinate system $ox_ty_{i_t}$ in the initial state, the spatial transformation of the coordinate system $ox_ty_tz_t$ to $ox'_wy'_wz'_w$ is realized when $ox_ty_tz_t$ is rotated around the x-axis by an angle α. The corresponding coordinate transformation matrix is:

$$M_\alpha = \begin{bmatrix} 1 & 0 & 0 \\ 0 & \cos\alpha & -\sin\alpha \\ 0 & \sin\alpha & \cos\alpha \end{bmatrix} \tag{1}$$

When $ox_t y_t z_t$ continues to rotate around the y-axis by an angle β, a spatial transformation of the coordinate system $ox'_w y'_w z'_w$ to $ox''_w y''_w z''_w$ is realized, and the corresponding coordinate transformation matrix is:

$$M_\beta = \begin{bmatrix} \cos\beta & 0 & \sin\beta \\ 0 & 1 & 0 \\ -\sin\beta & 0 & \cos\beta \end{bmatrix} \tag{2}$$

When $ox_t y_t z_t$ is then rotated by an angle γ around the z-axis, a spatial transformation of the coordinate system $ox''_w y''_w z''_w$ to $ox_w y_w z_w$ is realized, and the corresponding coordinate transformation matrix is:

$$M_\gamma = \begin{bmatrix} \cos\gamma & -\sin\gamma & 0 \\ \sin\gamma & \cos\gamma & 0 \\ 0 & 0 & 1 \end{bmatrix} \tag{3}$$

The coordinate rotation matrix M corresponding to the object coordinate system $ox_t y_t z_t$ to the reference coordinate system $ox_w y_w z_w$ can be obtained by multiplying the individual transformation matrices of a single transformation is denoted as:

$$\begin{aligned} M = M_\gamma M_\beta M_\alpha &= \begin{bmatrix} \cos\gamma & -\sin\gamma & 0 \\ \sin\gamma & \cos\gamma & 0 \\ 0 & 0 & 1 \end{bmatrix} \begin{bmatrix} \cos\beta & 0 & \sin\beta \\ 0 & 1 & 0 \\ -\sin\beta & 0 & \cos\beta \end{bmatrix} \begin{bmatrix} 1 & 0 & 0 \\ 0 & \cos\alpha & -\sin\alpha \\ 0 & \sin\alpha & \cos\alpha \end{bmatrix} \\ &= \begin{bmatrix} \cos\gamma\cos\beta & \cos\gamma\sin\alpha\sin\beta - \cos\alpha\sin\gamma & \sin\gamma\sin\alpha + \cos\gamma\cos\alpha\sin\beta \\ \cos\beta\sin\gamma & \cos\gamma\cos\alpha + \sin\gamma\sin\alpha\sin\beta & \cos\alpha\sin\gamma\sin\beta - \cos\gamma\sin\alpha \\ -\sin\beta & \cos\beta\sin\alpha & \cos\alpha\cos\beta \end{bmatrix} \end{aligned} \tag{4}$$

Similarly, the corresponding attitude angle of the object can be obtained by solving from the rotation matrix M as:

$$\begin{aligned} \alpha &= \arctan\left[\frac{M(3,2)}{M(3,3)}\right] \\ \beta &= -\arctan\left[\frac{M(3,1)}{\sqrt{M^2(3,2) + M^2(3,3)}}\right] \\ \gamma &= \arctan\left[\frac{M(2,1)}{M(1,1)}\right] \end{aligned} \tag{5}$$

The system first measures the field of view of the feature point through the attitude probe lead, so that the digital level meter can realize single-station measurement, avoiding the error of coordinate conversion and other errors existing in the current multi-station measurement method. On the basis of the real-time attitude of the object obtained by the combination system, the three-point distribution jacking of the attitude adjustment mechanism is adopted to realize the attitude adjustment of the object.

2.3.2. Attitude solver model

The definition and representation of each coordinate system of the attitude combination measurement system are shown in Fig. 3, in which o_1, o_2 and o_3 are the fixed characteristic points of the measured target. The local coordinate system of the digital level is $o_s x_s y_s z_s$, which is established with the center of the instrument as the origin, and the spatial translation relationship with the reference coordinate system, i.e., the axes of the two coordinate systems x, y and z are parallel respectively. According to the definition of object attitude, its pitch angle α_t, roll angle β_t are the rotation angle around the x_t -axis, y_t -axis, respectively. Sensor pitch angle α_q and roll angle β_q are rotation angles around x_q and y_q axes respectively.

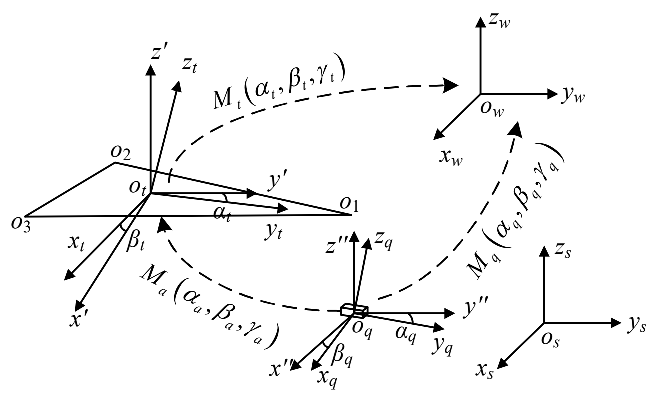

Fig. 3. Attitude combination measurement model coordinate system

According to the definition of each coordinate system and its transformation relationship, the transformation matrix between the reference coordinate system o_w, x_w, y_w, z_w, the local coordinate system of the measured object o_t, x_t, y_t, z_t and the local coordinate system of the inclination sensor o_q, x_q, y_q, z_q can realize the solution of the two horizontal attitude angles of the object, namely, the pitch angle and the roll angle.

According to the coordinate transformation theory, the transformation relationship between the sensor local coordinate system o_q, x_q, y_q, z_q and the reference coordinate system o_w, x_w, y_w, z_w is:

$$\begin{bmatrix} x_w \\ y_w \\ z_w \end{bmatrix} = M_q\left(\alpha_q, \beta_q, \gamma_q\right) \times \begin{bmatrix} x_q \\ y_q \\ z_q \end{bmatrix} + T_q \tag{6}$$

where M_q and T_q are the rotational translation matrices from the local coordinate system of the inclination sensor to the reference coordinate system. α_q, β_q, γ_q are the rotation angles around the x_q, y_q, z_q axes, respectively.

Similarly, the relationship between the local coordinate system of the inclination sensor o_q, x_q, y_q, z_q and the local coordinate system of the measured object o_t, x_t, y_t, z_t can be seen:

$$\begin{bmatrix} x_q \\ y_q \\ z_q \end{bmatrix} = M_a\left(\alpha_a, \beta_a, \gamma_a\right) \times \begin{bmatrix} x_t \\ y_t \\ z_t \end{bmatrix} + T_a \tag{7}$$

where M_a and T_a are the rotational translation matrices from the object coordinate system to the inclination sensor coordinate system, and α_a, β_a and γ_a are the rotation angles around the x_a, y_a and z_a axes, respectively.

Therefore, from Eqs. (6) and (7), the relationship between the local coordinate system o_t, x_t, y_t, z_t of the measured object and the reference coordinate system o_w, x_w, y_w, z_w is as follows:

$$\begin{bmatrix} x_w \\ y_w \\ z_w \end{bmatrix} = M_q\left(\alpha_q,\beta_q,\gamma_q\right)\times\left(M_a\left(\alpha_a,\beta_a,\gamma_a\right)\times\begin{bmatrix} x_t \\ y_t \\ z_l \end{bmatrix}+T_a\right)+T_q \tag{8}$$

From Eq. (8), the attitude rotation matrix from the local coordinate system o_t, x_t, y_t, z_t of the measured object to the reference coordinate system o_w, x_w, y_w, z_w is:

$$M_t\left(\alpha_t,\beta_t,\gamma_t\right)=M_q\left(\alpha_q,\beta_q,\gamma_q\right)\times M_a\left(\alpha_a,\beta_a,\gamma_a\right) \tag{9}$$

where M_t is the rotation matrix from the object coordinate system to the reference coordinate system, and α_t, β_t and γ_t are the rotation angles around x_t, y_t and z_t axes respectively. As can be seen from the above equation, after obtaining the rotation matrix M_t from the object coordinate system to the reference coordinate system, the real-time attitude angle of the object can be directly solved as:

$$\begin{aligned} \alpha_t &= \arctan\left(\frac{-\sin\beta_q v_1+\cos\beta_q\sin\alpha_q v_2+\cos\alpha_q\cos\beta_q\cos\beta_a\sin\alpha_a}{-\sin\beta_q v_3+\cos\beta_q\sin\alpha_q v_4+\cos\alpha_q\cos\beta_q\cos\alpha_a\cos\beta_a}\right) \\ \beta_t &= -\arcsin\left(-\sin\beta_q\cos\gamma_a\cos\beta_a\right. \\ &\quad \left.+\cos\beta_q\sin\alpha_q\cos\beta_a\sin\gamma_a-\cos\alpha_q\cos\beta_q\sin\beta_a\right) \end{aligned} \tag{10}$$

where α_t and β_t are the pitch and roll angles of the measured object, and α_a and β_a are fixed values, which can be obtained through pre-calibration. Therefore, the real-time attitude angle of the measured object can be obtained directly from the output angle of the inclination sensor itself.

From equation (9), the calibration matrix M_a can be obtained by solving the inverse of the measured target attitude and the inclination sensor attitude. The sensor attitude can be obtained from its own angle output. Next, the digital level is placed in front of the object within the height range where three probe scales can be observed simultaneously. The vertical heights of the feature points relative to the reference level are obtained by the digital level as $\left(h_1,h_2,h_3\right)$. Finally, the current static attitude of the target is obtained by spatial geometry:

$$\begin{aligned} \alpha_{ti} &= \arcsin\left(\frac{h_3-h_2}{l_c}\right) \\ \beta_{ij} &= \arcsin\left(\frac{2h_1l_c^2-h_2d_1-h_3d_2}{l_c\sqrt{4l_c^2l_a^2-d_1^2}}\right) \end{aligned} \tag{11}$$

where α_{ti}, β_{ti} are the pitch angle and roll angle of the object in the current attitude, $d_1=l_c^2+l_b^2-l_a^2$, $d_2=l_c^2+l_a^2-l_b^2$, l_a, l_b, l_c are the geometric distance parameters between feature points o_1 and o_2, o_1 and o_3, o_2 and o_3, respectively.

The real-time attitude angle α_{qi}, β_{qi}, α_{qi}, β_{qi} corresponding to its own in the object attitude of α_{ti}, β_{ti} is obtained from the output angle of the inclination sensor as the pitch and roll angles of the sensor, respectively, so that $M_b = M_a^{-1}$, according to Eq. (9), the calibration equation for M_b is obtained as:

$$\begin{cases} -\sin\beta_{ii}s_{11} + \cos\beta_{ii}\sin\alpha_{ii}s_{12} + \cos\alpha_{ii}\cos\beta_{ii}s_{13} = -\sin\beta_{qi} \\ -\sin\beta_{ii}s_{21} + \cos\beta_{ii}\sin\alpha_{ii}s_{22} + \cos\alpha_{ui}\cos\beta_{ii9}s_{23} = \cos\beta_{qi}\sin\alpha_{qi} \\ -\sin\beta_{ii}s_{31} + \cos\beta_{ii}\sin\alpha_{ii}s_{23} + \cos\alpha_{ti}\cos\beta_{i9}s_{33} = \cos\alpha_{qi}\cos\beta_{qi} \end{cases} \tag{12}$$

where s_{ij} is the i-row and j-column parameter of the rotation matrix M_b. There are 9 unknown parameters in the equation, and $n \geq 3$ sets of measured object attitudes are obtained using a digital level and combined with the real-time attitude angles from the inclination sensor. The matrix M_b can be obtained by least squares solution.

2.4. *Robust Integral Least Squares Methods*

The overall least squares method considers the fitting of data when the measurement coordinate points have errors in x, y, and z directions at the same time [25-26]. And this algorithm, on the basis of the overall least squares method, considers the case where there are errors or outliers in the data, and increases the accuracy and reliability of plane fitting by pre-excluding the abnormal data points in the data set through the outlier rejection algorithm.

Let the spatial plane equation of the measurement surface of the measurement target be Equation (13):

$$z = ax + by + c \tag{13}$$

Then the normal vector of the measured surface of the measuring target is $(a, b, -1)$. Where a, b, c are the parameters to be estimated.

The n three-dimensional point cloud data obtained from the data in the attitude measurement process are: $\{(x_i, y_i, z_i), i = 1, 2, 3, 4, \ldots, n\}$. Because the laser displacement sensor has a jump error and a certain measurement accuracy problem, as well as the experimental platform has an assembly error, etc., which will cause an error effect on the measurement data in all three coordinate directions. Therefore, it is assumed that the three-dimensional point cloud data have errors in each of the three directions X, Y, and Z, and the equation can be expressed as Eq. (14):

$$z_{\mathrm{i}} + v_{z_i} = a\left(x_i + v_{x_i}\right) + b\left(y_i + v_{y_i}\right) + c \tag{14}$$

where v_{x_i}, v_{y_i} and v_{z_i} are the error correction numbers in the directions X, Y and Z respectively. The above equation is organized to obtain equation (15):

$$\left(A + E_A\right)x = L + E_L \tag{15}$$

where E_A and E_L denote the error in the measurement of matrix A and vector L, respectively, as indicated by Eq. (16):

$$\underset{n,3}{A}=\begin{bmatrix} x_1 & y_1 & 1 \\ x_2 & y_2 & 1 \\ \hat{\partial} & \dot{\partial} & \dot{\partial} \\ x_n & y_n & 1 \end{bmatrix}, \underset{n,3}{E_A}=\begin{bmatrix} v_{x_1} & v_{y_1} & 1 \\ v_{x_2} & v_{y_2} & 1 \\ \dot{\partial} & \dot{\partial} & \dot{\partial} \\ v_{x_n} & v_{y_n} & 1 \end{bmatrix}$$
$$x,1=\begin{bmatrix} a \\ b \\ c \end{bmatrix}, \underset{n,1}{z}=\begin{bmatrix} z_1 \\ z_2 \\ \dot{\partial} \\ z_n \end{bmatrix}, \underset{n,1}{E_L}=\begin{bmatrix} v_{z_1} \\ v_{z_2} \\ \dot{\partial} \\ v_{z_n} \end{bmatrix} \tag{16}$$

Noting the augmented matrix $\begin{bmatrix} A & L \end{bmatrix}$, the matrix singular value decomposition (SVD) method can be used to solve the overall least squares solution for the parameters to be determined, as in Eq. (17):

$$\begin{bmatrix} A & L \end{bmatrix} = U\Sigma V^T \tag{17}$$

and:

$$V^T=\begin{bmatrix} V_{11} & V_{12} \\ V_{21} & V_{22} \end{bmatrix} \tag{18}$$

where T denotes the conjugate transpose, U and V are You matrices, $U=(u_1,u_2,u_3,u_4)$, $U \in R^{n\times 4}$, and Σ denote nonnegative diagonal matrices, $\Sigma \in R^{4\times 4}$, $V_{11} \in R^{3\times 3}$, $V_{12} \in R^{3\times 1}$, $V_{21} \in R^{1\times 3}$, and $V_{22} \in R^{1\times 1}$. Then the overall least squares estimate of the parameters can be expressed as Equation (19):

$$x=-V_{12}V_{22}^{-1} \tag{19}$$

The distance from the point to the fitting plane is as in equation (20):

$$d_i=\frac{|ax_i+by_i-z_i+c|}{\sqrt{a^2+b^2+1}}, (i=1,2,\Lambda,n) \tag{20}$$

The average distance $\bar{d}$ of all point cloud data from the fitting plane can be expressed as equation (21):

$$\bar{d}=\frac{\sum_{i=1}^{n} d_i}{n} \tag{21}$$

The standard deviation of the distance from each point to the plane is given by equation (22):

$$\hat{\sigma}=\sqrt{\frac{\sum_{i=1}^{n}\left(d_i-\bar{d}\right)^2}{n-1}} \tag{22}$$

The plane fitting accuracy is represented by Eq. (23):

$$\hat{\sigma}_p=\sqrt{\frac{\sum_{i=1}^{n} d_i^2}{n}}, (i=1,2,\Lambda,n) \tag{23}$$

In the actual attitude measurement of the target object, it is inevitable that due to various factors, such as other objects interfering with the laser path, laser displacement sensor data jumps, etc., there will inevitably be data points in the collected data that are different from the real value. And these data points will seriously affect the accuracy of the target object attitude measurement. Therefore, in order to improve the robustness and measurement accuracy of the measurement system, when the overall least squares method is used to fit the spatial plane, the data set is subjected to outlier rejection in order to obtain robust estimates of the plane parameters a, b, and c. The specific algorithm is as follows:

1) Calculate initial estimates of a, b, c for all 3D point cloud data using each of the three plane fitting methods.

2) Calculate the distance d_i from each point to the initial fitting plane based on the calculated estimate of a, b, c.

3) Calculate the standard deviation of the distance d_i.

4) Set the rejection threshold to 3σ. When $d_i > 3\sigma$, the point is considered to be an anomaly and is removed from the point cloud data. When $d_i <= 3\sigma$, the point is retained as valid point cloud data.

5) Eliminate the anomalous points by iterating for a certain number of times, which is set to 20 times in this paper.

6) Using the eliminated point cloud data, the algorithm calculates the estimated values of parameters a, b, and c, i.e., the best planar parameter estimates are obtained.

3. Attitude measurement algorithm simulation validation

By building a binocular stereo vision measurement system to control the camera to capture the checkerboard grid calibration board, the semi-transparent simulated flight target, and the simulated flight target with auxiliary markers, respectively, to complete the acquisition of experimental images. And based on Matlab platform combined with OpenCV vision library for software design, the algorithm processing of experimental images is completed. The measurement results of system calibration, flight target attitude and rotational speed are further obtained to verify the feasibility of the method in this paper. Accuracy analysis is carried out for the measurement error of the system, and comprehensive error analysis is carried out based on the measurement results of flight target attitude and rotational speed, and experimental verification of the measurement results is carried out to verify the effectiveness of the system in this paper.

According to the needs of the engineering projects involved in this paper, the measurement system mainly has the following technical indexes:

1) Camera reprojection error: ≤ 0.5 pixels.

2) Pitch angle measurement error: $\pm 0.75°$.

3) Yaw angle measurement error: $\pm 0.75°$.

4) Rotation speed measurement error: $< 5\%$.

3.1. Measurement experiment design

3.1.1. Design of the overall flow of the experiment. The overall flow design of the experiment includes the following aspects:

1) Measurement system construction: build the experimental platform of binocular stereo vision measurement system.

2) Experimental Image Acquisition: Control the binocular camera to acquire the experimental images, including the calibration plate image and two simulated flight target images.

3) Measurement system calibration: process the collected calibration plate images through the binocular camera calibration algorithm, and complete the calibration of the internal and external parameters of the two cameras, the aberration parameters of the two lenses and the external parameters of the system.

4) Flight Target Attitude Measurement: Process the semi-transparent simulated flight target image through the motion target detection and image post-processing algorithm, and combine with the

center-axis solving method to complete the measurement of the flight target attitude (pitch angle and yaw angle).

5) Measurement of flight target rotational speed: The image mask and image preprocessing algorithm are used to process the simulated flight target image with auxiliary flags, and combined with the auxiliary flag solving method to complete the measurement of flight target rotational speed (spin angle).

6) Measurement result analysis: Based on the accuracy analysis of binocular stereo vision measurement system, comprehensive error analysis is carried out on the system calibration, flight target attitude and rotational speed measurement results.

3.1.2. Experimental platform construction and software design. The experimental platform for the binocular stereo vision measurement system actually built in this paper mainly consists of two VEO1310L high-speed cameras, two AF NIKKOR 35mm lenses, a GP400 black-and-white checkerboard grid calibration board, and two simulated flying targets (semi-transparent and marked).

In order to validate the flight target attitude and rotational speed measurement method given in this paper, and to facilitate the accuracy error analysis of the measurement results. In the actual experimental process, the following experimental conditions or parameters in the measurement system are constrained or calibrated in this paper.

1) Size of measurement area: 500mm(L)*300mm(H)*300mm(W).

2) Distance between the center of the measurement area and the ground: 1.35m.

3) Baseline distance: 2.15m.

4) Camera focal length: 35mm.

5) Angle between optical axis and baseline.

Among them, the camera focal length is known, and the parameters such as baseline distance, optical axis and baseline angle are obtained through camera calibration.

This paper is based on Matlab platform combined with OpenCV vision library for software design. The algorithmic processing of the experimental images is completed around four parts: calibration, target detection, attitude solving and rotational speed measurement.

3.2. Target Spatial Position and Attitude Measurement Experiments

3.2.1. System Stability Experiments. The main purpose of the system stability experiment is to verify the accuracy of the data acquired by the equipment of this system. The higher the data stability represents the more the data can reflect the correct degree of the measured data.

The experiment is mainly carried out through the timed acquisition function set in the MFC of the host computer, that is, every time the acquisition button is clicked, the system will continuously acquire data for 100 flash cycles.

The timing function is completed by the multimedia timer timeSetEvent function, which is characterized by high precision compared with the WM_TIME timer that comes with MFC.

In the experiment, the timing time is set to 3ms, the timing accuracy is 1ms, and the flash feature point period is set to 10ms, that is to say, the number of valid 100 samples is collected in 1s time.

The main factors affecting the stability of the system for the detector data obtained by the signal-to-noise ratio, the detection distance of the distance affects the size of the effective signal, which will change the size of the stability of the system. In this paper, we analyze the stability of the system based on the experimental data obtained by conducting detection experiments at distances of 5m, 10m, 15m, and 20m, respectively.

The scatter distribution of system stability at different distances is shown in Fig. 4. The figure gives the scatter plot of the distribution of the data of the leveling process among 100 groups of target data obtained in the process of timing acquisition. The blue scatter, green scatter, yellow and pink scatter represent the data distribution at 5m, 10m, 15m and 20m respectively.

From the figure, it can be seen that the stability of the detection system itself decreases with the increase of distance. The 90% confidence intervals at 5m, 10m, 15m, and 20m are [-3.21mm, 3.56mm], [-9.87mm, 12.17mm], [-18.02mm, 15.23mm], and [-26.25mm, 23.74mm], which is consistent with the fact that the system operates at a long distance with a reduced effective optical signal and a reduced signal-to-noise ratio, resulting in a design is characterized by large fluctuations in the detected data.

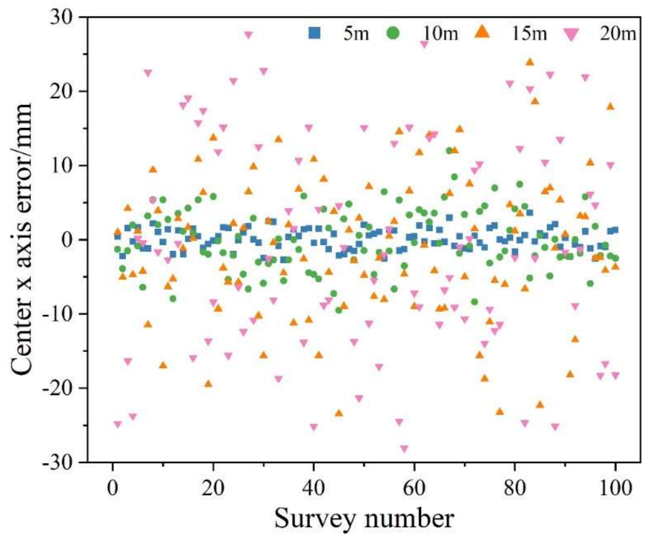

Fig. 4. The system stability dispersion point distribution in different distance

3.2.2. System Accuracy Test Experiment. The stability of the detection system indicates the magnitude of the signal-to-noise ratio of the system during the detection process. In connection with the accuracy requirements in the program design, this paper obtains the data of translation, roll and deflection direction at 5m, 10m, 15m and 20m respectively by designing experiments. The distribution of system accuracy at different distances is shown in Fig. 5. The standard deviation of the measurement system shows a positive correlation between the standard deviation of the measurement system and the detection distance, which also shows the higher accuracy of the real-time data obtained by the system stabilization when the system is performing close detection.

Figure (a) shows the image of the standard deviation distribution obtained when the experimental system is subjected to a spatial movement operation. The accuracy of the translation at 20m required in the comparison program is 10cm, and the accuracy of this system reaches 12.79056mm, which fully meets the requirement of accuracy in detection.

Figure (b) is the standard deviation distribution image of the deflection data in the experimental data. Among them, the accuracy at 20m reaches 1.45969°, and the experimental results are better than the 3° required in the system program.

Figure (c) gives the distribution image of the pitch angle in the experimental data, from which it can be seen that an accuracy of 1.33401° is achieved at 20m detection distance. Theoretically, in the data given in this experiment, the two have some differences, but the general results are similar. This result shows the correctness of the data collected by this system.

Figure (d) is the standard deviation distribution image of the roll angle data in the experimental data. 5m and 20m detection accuracy is 0.32663° and 3.86557° respectively, which is lower than the 5° detection requirement of the system.

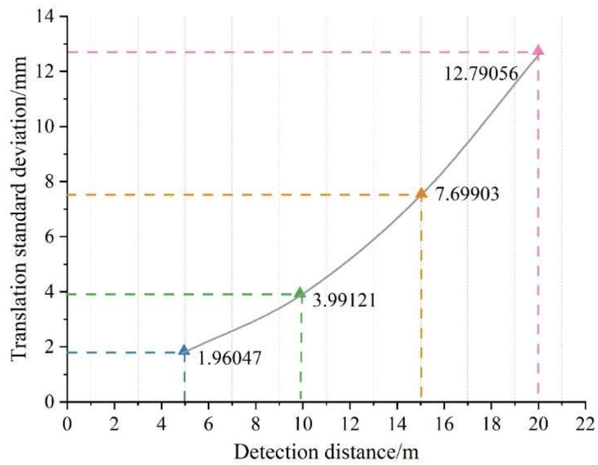

(a) Translation

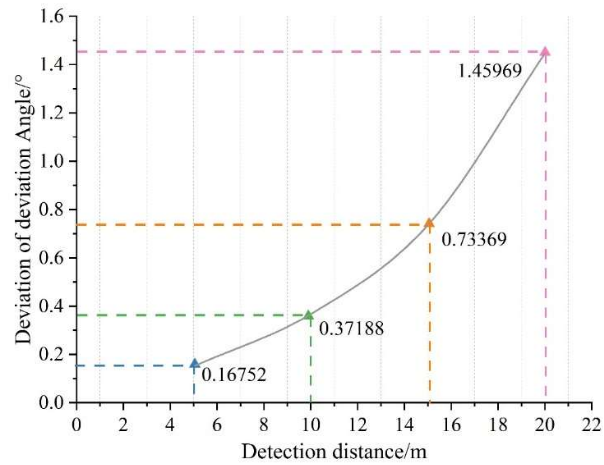

(b) Yaw Angle

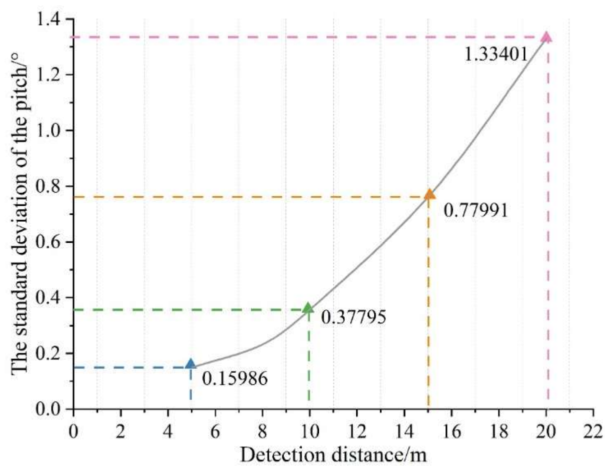

(c) Pitch Angle

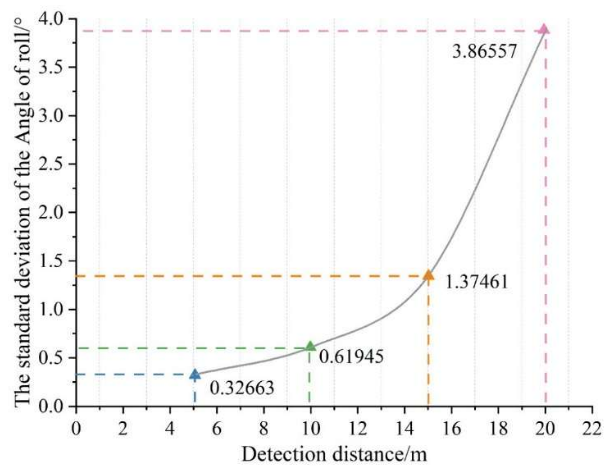

(d) Rolling Angle

Fig. 5. The distribution of system accuracy in different distances

3.2.3. Target Position Measurement Experiments. Due to the large size of the target indication unit during the experiment, the direct movement error is high. In this paper, by fixing the measured target indication unit in the remote position, the photoelectric detection unit is fixed on the motor platform with the function of translation and deflection for the relevant movement and experiment.

1) Panning state. Place the target indicator unit at 5m, 10m, 15, 20m respectively and fix it, and place the photoelectric detection unit on the displacement platform. The photoelectric detection unit was moved along the horizontal direction at equal intervals, and the detector piece was moved 210mm at 10mm intervals.

Linear fitting was performed on the data in each of the four cases, and the system translational response images at different distances are shown in Fig. 6. Among them, Fig. (a) is the measurement results at 5m and 10m, and Fig. (b) is the measurement results at 15m and 20m distances. From the figure, it can be seen that the system shows a linear relationship between the response position of the system and the actual moving position in the translational state. The measured data obtained at 5m is the most linear, and the degree of linearity of the obtained data becomes weaker as the distance increases.

Linear error analysis of the measured target data at several distances, after calculation in the 20m detection distance detection system translational linear error within 0.742%, very close to its own typical nonlinear error of 0.27%.

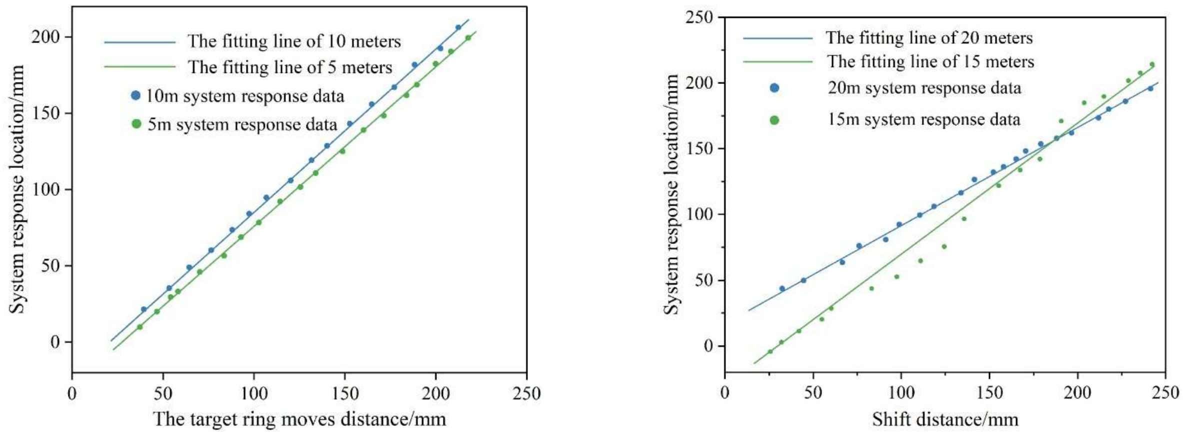

(a) Measurements of 5m,10m (b) Measuring results of 15m,20m distance

Fig. 6. The system translational response image from different distances

2) Deflection state. In order to study the response results of the system in the deflection state, the photoelectric detection unit was placed on the rotating motor platform and the target indication unit was placed at a distance of 5m. The photoelectric detection unit was rotated at equal angles along the axis position, with a rotation range of 40 degrees and a rotation interval of 10 degrees. The results of the system deflection angle response at a distance of 5m were obtained. It can be found that as the deflection angle increases, the accuracy of the deflection angle response becomes better and better.

3.3. Simulation of attitude measurement system based on multi-sensor combination

3.3.1. Simulation test preparation. In order to verify the accuracy and validity of the attitude measurement system in this paper, simulation experiments will be launched in this chapter for verification. Initially, the attitude simulation in dynamic situation is verified based on Witte Intelligent JY931 (integrated three-axis gyroscope, three-axis accelerometer and three-axis magnetometer).

JY931 can output angular velocity, acceleration, magnetic field strength and reference angle information, and take the angular velocity, acceleration and magnetic field strength output from JY931 as the inputs of the attitude measurement algorithm introduced in this paper, and solve to get the attitude angle information. And the attitude angles obtained by different algorithms are compared and analyzed with the reference attitude angle output from JY931, so as to verify the effectiveness of the attitude measurement system based on the combination of multi-sensors designed in this paper.

3.3.2. Dynamic Simulation Verification. In the dynamic experimental test, under the condition of room temperature, the JY931 module was rotated by handholding, so that it outputs dynamic data, and the sampling frequency was set to 100 Hz, and the sampling interval was Δt =0.02s.

The dynamic test results of JY931 are shown in Fig. 7, and the angular velocity, acceleration, and magnetic field strength information output by JY931 are shown in Fig. (a). At the same time, JY931 outputs the rotating Euler angles, i.e., traverse roll angle, pitch angle, and heading angle, as shown in Fig. (b).

The angular velocity, acceleration, and magnetic field strength of JY931 output are [-20,20], [-2,2], and [-3,1], respectively.

The roll angle, pitch angle, and heading angle of JY931 are [-20,20], [-20,20], and [-2,6], respectively.

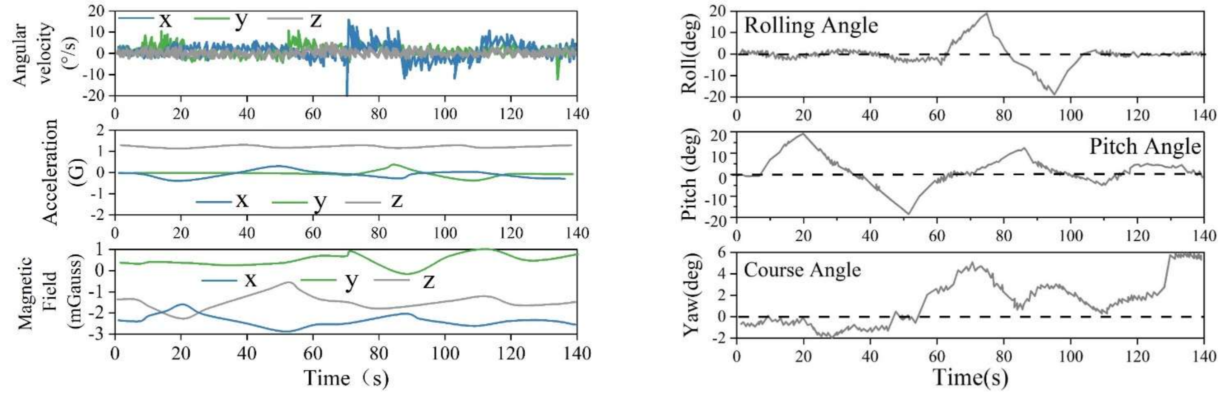

(a) Angular velocity, acceleration, magnetic field intensity (b) Angle of rolling Angle, pitch Angle, course Angle

Fig. 7. Dynamic test results for jy931

Similarly, after the dynamic data acquisition, the algorithm is simulated and verified on the MATLAB platform.

Mahony algorithm, FKF algorithm, UKF algorithm and the attitude solution model used in this paper are used to solve the JY931 output angular velocity, acceleration, magnetic field strength information to obtain the rotating attitude angle.

The results of the roll angle measurement are shown in Fig. 8, Fig. (a) and Fig. (b) show the roll angle solved by several algorithms, and the roll angle measurement error, respectively. The change curves of the four algorithms of the roll angle are basically the same at the measurement time, but the measurement error of the roll angle of the UKF algorithm is larger, and the fluctuation range of the error is -3~2. The roll angle error of the algorithm in this paper is concentrated in the interval of [-1,1], and the fluctuation ups and downs are relatively small.

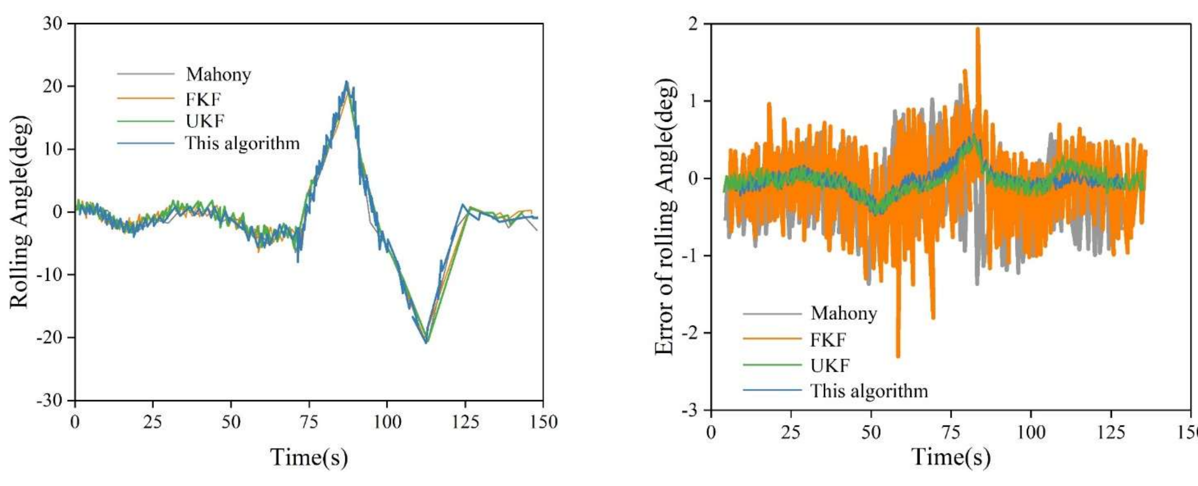

(a) Rolling Angle (b) Error of measurement of rolling Angle

Fig. 8. Rolling Angle measurement results

The pitch angle and pitch angle measurement errors solved by the four algorithms under dynamics are shown in Fig. 9. Figures (a) and (b) show the pitch angle and pitch angle measurement errors at the solutions of Mahony algorithm, FKF algorithm, UKF algorithm and the algorithm of this paper, respectively. From Fig. (b), it can be seen that the pitch angle error obtained from the attitude solving model applied in this paper is the smallest, and there is a large fluctuation in the measurement time of 50~100s, but the error is always controlled within the range of [-1,1].

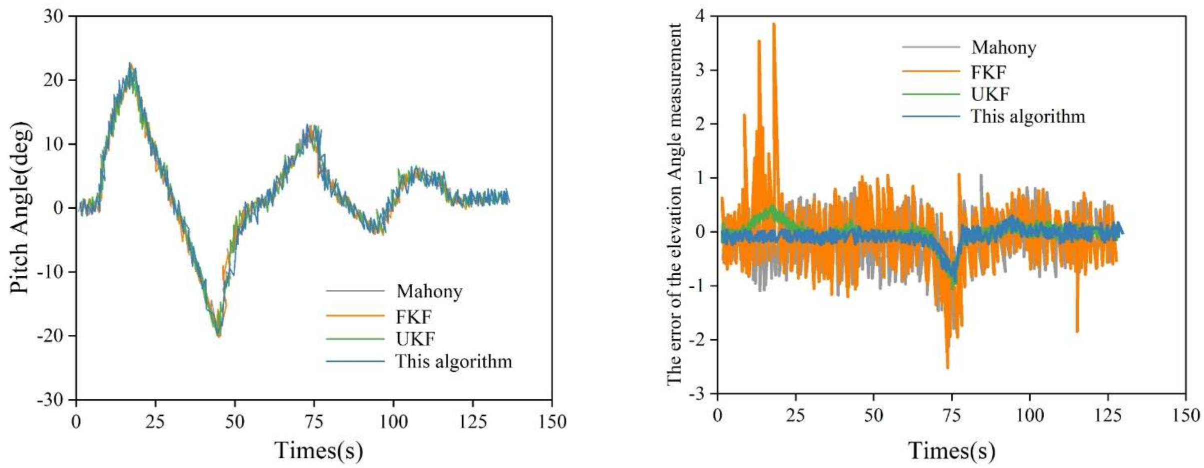

(a) Pitch Angle (b) The error of the elevation Angle measurement

Fig. 9. Angle and pitch measurement error

The heading angles and heading angle measurement errors solved by the four algorithms under the dynamics are shown in Fig. 10, and Figs. (a) and (b) show the heading angles solved by different algorithms and the heading angle measurement errors, respectively.The measurement errors of the UKF algorithm for the heading angles show large fluctuations in the measurement time of 50~100s, and the measurement errors are in the range of -2~6.

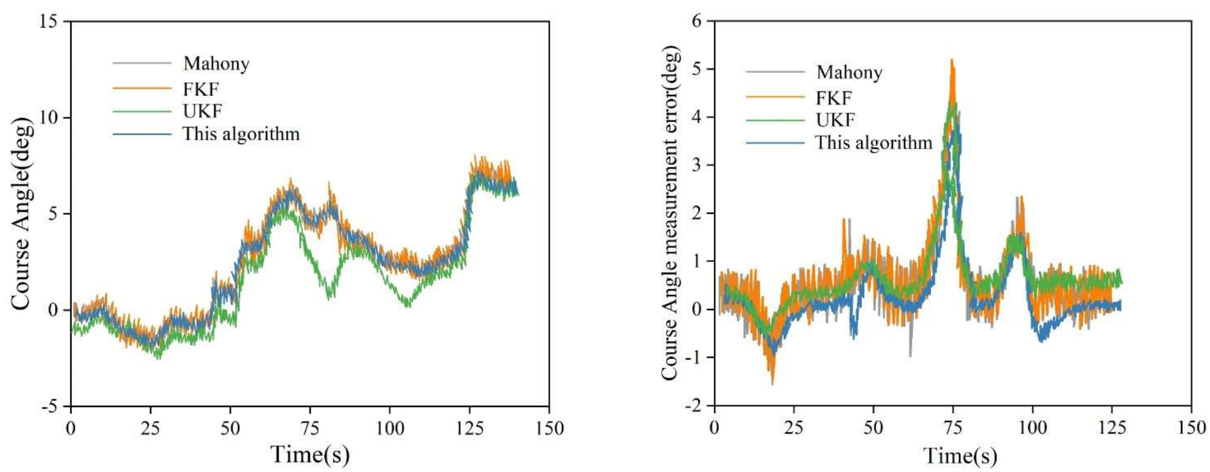

(a) Course Angle (b) Course Angle measurement error

Fig. 10. The measurement error of course Angle and heading Angle in motion

Based on the dynamic attitude measurement results of the above algorithms, the root mean square error (RMSE) between them and the reference attitude angle is calculated respectively, and the RMSE (degrees) of the attitude angle under dynamic is shown in Table 1.

The data in the table shows that the RMSEs of the roll, pitch, and heading angles measured by the algorithm in this paper are 0.2982, 0.2214, and 1.0333, respectively.The RMSEs of the attitude measurements in the dynamic case are larger, which is due to the fact that the noise and uncertainty in the measurement process may become more significant in a dynamic system, and the rapidly changing attitude may lead to the discontinuity of the sensor data or inaccuracy, which increases the error of attitude measurement.

Table 1. Balance of the attitude Angle of the dynamic Angle (degree)

Algorithm/attitude Angle	RMSE		
	Rolling Angle	Pitch Angle	Course Angle
Mahony	0.5236	0.3624	1.3625
FKF	0.3517	0.2245	1.1123
UKF	0.4043	0.3659	1.3967
This algorithm	0.2982	0.2214	1.0333

4. Conclusion

This paper analyzes the structure of aircraft landing impact test and designs the impact platform simulation. It proposes a space attitude measurement system based on multi-sensor combination, analyzes the attitude solution model, and uses the robust integral least squares method for plane fitting to find the attitude angle during the aircraft landing impact.

The maximum design load is calibrated by finite elements, and the impact platform is designed according to 1.25 times of the safety system. The static finite element calibration of the strength of the nuclear test system shows that the maximum yield strength is 345 MPa, and the impact test calibration shows that the maximum impact stress of the platform is about 250 MPa. Considering the transient impact load, the impact platform is able to meet the requirements of load carrying as well as the requirements of the impact overload in the case of emergency landing.

The 90% confidence interval of the multi-sensor combination-based space attitude measurement system at 5m is [-3.21mm, 3.56mm], and its stability meets the target space measurement requirements. The accuracy reaches 12.79056mm, which fully meets the requirement of accuracy in detection. The attitude solution model used in this paper finds that the measurement errors of the roll angle, pitch angle and heading angle as well as the root-mean-square error of JY931 under the dynamic experimental test are smaller, which is more in line with the space attitude measurement.

Support Fund

This project is supported by Chinese Aviation Science Foundation: Application of Artificial Intelligence in Landing Gear Dynamics (No.2023M009023006).

References

[1] Orkisz, M., & Kuźniar, M. (2020). 3E-A new paradigm for the development of civil aviation. Combustion Engines, 59(2).

[2] Zhou, C. (2025). Development Expectation Gap of Design-Build Contract Delivery in China's Civil Aviation Infrastructure Projects. Archives of Advanced Engineering Science, 3(1), 51-60.

[3] Mostafa, A. (2020). Safety and risk assessment of civil aircraft during operation. Safety and Risk Assessment of Civil Aircraft during Operation.

[4] Enrico, Z. I. O., Mengfei, F. A. N., Zhiguo, Z. E. N. G., & Rui, K. A. N. G. (2019). Application of reliability technologies in civil aviation: Lessons learnt and perspectives. Chinese Journal of Aeronautics, 32(1), 143-158.

[5] Wang, H., Wu, D., Wang, F., & Ren, H. (2018). A method for determining the horizontal impact load based on the rotational speed of the aircraft's wheel in a landing gear drop test. International journal of crashworthiness, 23(6), 627-634.

[6] Liu, W., Wang, Y., & Ji, Y. (2023). Landing Impact Load Analysis and Validation of a Civil Aircraft Nose Landing Gear. Aerospace, 10(11), 953.

[7] Jackson, K. E., & Fasanella, E. L. (2016, June). Crash Testing and Simulation of a Cessna 172 Aircraft: Hard Landing Onto Concrete. In International LS-DYNA Conference (No. NF1676L-22884).

[8] Perfetto, D., De Luca, A., Lamanna, G., Chiariello, A., Di Caprio, F., Di Palma, L., & Caputo, F. (2018). Drop test simulation and validation of a full composite fuselage section of a regional aircraft. Procedia Structural Integrity, 12, 380-391.

[9] Gan, Y., Fang, X., Wei, X., & Nie, H. (2021). Numerical and experimental testing of aircraft tyre impact during landing. The Aeronautical Journal, 125(1294), 2200-2216.

[10] Bronstein, M., Feldman, E., Vescovini, R., & Bisagni, C. (2015). Assessment of dynamic effects on aircraft design loads: The landing impact case. Progress in Aerospace Sciences, 78, 131-139.

[11] Ali, S., Fawzia, S., Thambiratnam, D., Liu, X., & Remennikov, A. M. (2020). Performance of protective concrete runway pavement under aircraft impact loading. Structure and Infrastructure Engineering, 16(12), 1698-1710.

[12] Zhicong, L., & Voronko, I. (2023). AIRCRAFT LANDING GEAR TEST FOR EMERGING LOADS. GRAIL OF SCIENCE.

[13] Wang, T., Dong, Z., Cao, C., Zhou, J., Meng, Y., & Quan, W. (2024). Characterization of aircraft landing impact loads: Effects on vertical tire-pavement contact characteristics and pavement performance. Construction and Building Materials, 457, 139365.

[14] Sadique, M. R., Iqbal, M. A., & Bhargava, P. (2022, May). Aircraft-structure interaction study for the assessment of the reaction-time response of nuclear containment structure. In Structures (Vol. 39, pp. 866-881). Elsevier.

[15] Tavares, S. M. O., & De Castro, P. M. S. T. (2017). An overview of fatigue in aircraft structures. Fatigue & Fracture of Engineering Materials & Structures, 40(10), 1510-1529.

[16] Lopresto, V. (2022). Impact induced dynamic response and failure behavior of aircraft structures. Progress in Aerospace Sciences, 129, 100792.

[17] Yuan, S., Ren, Y., Qiu, L., & Mei, H. (2016). A multi-response-based wireless impact monitoring network for aircraft composite structures. IEEE Transactions on Industrial Electronics, 63(12), 7712-7722.

[18] Zimmermann, N., & Wang, P. H. (2020). A review of failure modes and fracture analysis of aircraft composite materials. Engineering failure analysis, 115, 104692.

[19] Sudatham, W., Matsumoto, H., Takahashi, S., & Takamasu, K. (2016). Non-contact measurement technique for dimensional metrology using optical comb. Measurement, 78, 381-387.

[20] Wu, T., Tang, L., Du, P., Liu, N., Zhou, Z., & Qi, X. (2022). Non-contact measurement method of beam vibration with laser stripe tracking based on tilt photography. Measurement, 187, 110314.

[21] Chen, H., Ren, Y., Gan, S., Li, Y., Wang, J., & Nie, X. (2024, April). Interfacial debonding detection for steel-concrete composite structures part I: Benchmark test and signal calibration of contact and non-contact measurement. In Structures (Vol. 62, p. 106123). Elsevier.

[22] Lezhin, D. S., Falaleev, S. V., Safin, A. I., Ulanov, A. M., & Vergnano, D. (2017). Comparison of different methods of non-contact vibration measurement. Procedia Engineering, 176, 175-183.

[23] Tongxu Wang,Zejiao Dong,Cheng Cao,Jie Zhou,Yuhang Meng & Weiwen Quan. (2024). Characterization of aircraft landing impact loads: Effects on vertical tire-pavement contact characteristics and pavement performance. Construction and Building Materials139365-139365.

[24] Haosu Zhang,Zihao Wang,Shiyin Zhou,Cheng Ma,Sheng Wang,Fafu Zhang & Lingji Xu. (2024). Underwater Horizontal Attitude Determination Technology Based on Fusion Power Circle Theory and Improved 3D Cone Hough Transform. Electronics(23),4689-4689.

[25] Tobias Seger,Christoph Menke,Matthias Sonntag & Karsten Urban. (2025). Efficient evaluation of the Jacobian in the damped least-squares method for optical design problems using algorithmic differentiation.. Optics express(2),3054-3067.

[26] Samuel J. Harris & N.R. McDonald. (2025). Modelling wildfire spread and spotfire merger using conformal mapping and AAA-least squares methods. Environmental Modelling and Software106303-106303.